Long-Range Strain Correlations in Sheared Colloidal Glasses

Vijayakumar Chikkadi,[1] Gerard Wegdam,[1] Daniel Bonn,[1] Bernard Nienhuis,[2] and Peter Schall[1]

[1]*Van der Waals-Zeeman Institute, University of Amsterdam, Science Park 904, 1098 XH Amsterdam, The Netherlands*
[2]*Institute for Theoretical Physics, University of Amsterdam, Science Park 904, 1098 XH Amsterdam, The Netherlands*

Glasses behave as solids on experimental time scales due to their slow relaxation. Growing dynamic length scales due to cooperative motion of particles are believed to be central to this slow response. For quiescent glasses, however, the size of the cooperatively rearranging regions has never been observed to exceed a few particle diameters, and the observation of long-range correlations has remained elusive. Here, we provide direct experimental evidence of long-range correlations during the deformation of a dense colloidal glass. By imposing an external stress, we force structural rearrangements, and we identify long-range correlations in the fluctuations of microscopic strain and elucidate their scaling and spatial symmetry. The applied shear induces a transition from homogeneous to inhomogeneous flow at a critical shear rate, and we investigate the role of strain correlations in this transition.

Glasses have attracted considerable attention due to their ubiquity in nature and for the scientific challenges they pose [1]. Because of their long relaxation time, glasses behave as solids on experimental time scales; this slow response is often attributed to cooperative motion of particles [2]. Dynamic correlations that are used to characterize the length scales of the cooperatively rearranging regions are indeed observed to grow on approach to the glass transition [3,4]. However, despite the rapid growth of the glass relaxation time and the glass viscosity by many orders of magnitude, the length scale associated with the dynamic correlations increases only weakly on approach to the glass transition. Simulations as well as experiments have shown that, in quiescent glasses, the dynamic length scales remain limited to a few particle diameters [3,4]. On the other hand, recent simulations on driven, athermal amorphous materials have evidenced the existence of avalanchelike, long-range correlated flow [5]. Correlations in slowly driven thermal glasses, however, are poorly explored. Here, we show that even a glass exhibits long-range correlations in the microscopic flow field when it is driven so slowly that the rearrangements induced by the flow happen on a time scale similar to that of the spontaneous (thermal) rearrangements. By imposing very slow shear, we explore the transition from a regime where the spontaneous fluctuations are sufficiently rapid to accommodate the flow to a regime where this is no longer possible, and this allows us to probe long-range correlations. Nevertheless, in strained molecular glasses, direct observation of such correlations is prohibitively difficult, because the small size of molecules inhibits direct observation. We therefore use direct real-space observation in suspensions of colloidal particles; the individual particles can be imaged and their motion be tracked accurately in three dimensions with confocal microscopy [6]. Hard-sphere colloidal suspensions have become a

much-used model system for studying glasses; at high packing densities, the motion of the colloidal particles becomes increasingly frustrated, and structural relaxations slow down dramatically at particle volume fractions larger than $\phi_g \sim 0.58$, the colloidal glass transition [7]. By taking advantage of recent imaging techniques to image large sample volumes containing as many as $\sim 2.5 \times 10^5$ particles, we show that the flow of glasses is governed by surprisingly long-range correlations.

We follow correlations in the deformation of the glass directly in three dimensions and real time by visualizing fluctuations in the microscopic strain and nonaffine displacements. These strain fluctuations exhibit remarkably long-range correlation that extend over the full system size, far beyond the range of dynamic correlations reported for quiescent glasses. [3,4]. We investigate these correlations during two different modes of macroscopic deformation: during homogeneous flow at very low applied shear rates $\dot{\gamma}$ much smaller than the inverse structural relaxation time τ^{-1} of the glass and during inhomogeneous flow at strain rates $\dot{\gamma} > \tau^{-1}$. These two modes of deformation are also observed for molecular glasses [8], and the direct visualization of strain fluctuations allows us to identify their important role in the transition between both modes. Surprisingly, we find that the scaling behavior of the strain correlations is uniform over the investigated range of shear rates, suggesting a robust, scale-free organization of the flow of glasses.

We used sterically stabilized fluorescent polymethylmethacrylate particles suspended in a density and refractive index matching mixture of cycloheptyl bromide and *cis*-decalin. The particles have a diameter of $\sigma = 1.3$ μm, with a polydispersity of 7% to prevent crystallization. A colloidal glass with a volume fraction of $\phi \sim 0.60$ is prepared by diluting samples centrifuged to a sediment with $\phi \sim 0.64$. The suspension is loaded in a cell between

two parallel plates a distance of 65 μm apart. Boundary-induced crystallization is suppressed by a layer of polydisperse particles on the plates. We used a piezoelectric translation stage to move the top plate to apply shear at very slow rates between $\dot{\gamma} = 10^{-5}$ s^{-1} and $\dot{\gamma} = 10^{-4}$ s^{-1}, of the order of the inverse structural relaxation time of the glass. We used confocal microscopy to image individual particles in a 107 μm by 107 μm by 65 μm volume and determined their positions in three dimensions with an accuracy of 0.03 μm in the horizontal and 0.05 μm in the vertical direction [6]. We tracked the motion of $\sim 2 \times 10^5$ particles during a 25 min time interval by acquiring image stacks every 60 s. The mean square displacement $\langle \Delta r^2 \rangle$ of particles in the quiescent glass is shown in Fig. 1(a); we estimate the structural relaxation time of the glass $\tau \sim 2 \times 10^4$ s from the requirement $\langle \Delta r(\tau)^2 \rangle = (\sigma/2)^2$; this relaxation time is a factor of 5×10^4 larger than the Brownian relaxation time at infinite dilution, $\tau_B = 0.4$ s. Because the hard-sphere glass exhibits aging, this structural relaxation time changes with time. To obtain reproducible results, all measurements presented here were taken consistently ~ 3 h after mechanical rejuvenation of the sample.

We study correlations in the deformation of the glass by decomposing the particle motion into affine and nonaffine components. To do so, we follow particle trajectories and identify the nearest neighbors of each particle as those separated by less than r_0, the first minimum of the pair correlation function. We subsequently determine the best affine deformation tensor $\boldsymbol{\Gamma}$ describing the transformation of the nearest neighbor vectors, $\mathbf{d_i}$, over the time interval δt [9], by minimizing $D_{\min}^2 = (1/n) \sum_{i=1}^{n} [\mathbf{d_i}(t + \delta t) - \boldsymbol{\Gamma}\mathbf{d_i}(t)]^2$. The symmetric part of $\boldsymbol{\Gamma}$ is the local strain tensor. The remaining nonaffine component $D_{\min}^2$ has been used as a measure of plastic deformation [9]. We define correlations in the fluctuations of the principal shear strain component ϵ_{xz} and the nonaffine displacement $D_{\min}^2$ by using

$$C_A(\delta \mathbf{r}) = \frac{\langle A(\mathbf{r} + \delta\mathbf{r})A(\mathbf{r}) \rangle - \langle A(\mathbf{r}) \rangle^2}{\langle A(\mathbf{r})^2 \rangle - \langle A(\mathbf{r}) \rangle^2}, \quad (1)$$

where $A = \epsilon_{xz}$ or $A = D_{\min}^2$ and angular brackets denote ensemble averages. C_A correlates values of ϵ_{xz} or $D_{\min}^2$ at locations separated by $\delta \mathbf{r}$.

We investigate strain correlations during homogeneous flow of the glass by subjecting the glass to a shear rate of $\dot{\gamma} \sim 1.5 \times 10^{-5}$ s^{-1}, a factor of 6 smaller than the inverse structural relaxation time. At this shear rate, thermally activated relaxation occurs sufficiently fast, and after an initial transient the colloidal glass flows homogeneously. We shear the glass to $\gamma \sim 1$ to address steady-state flow and show the displacements Δx of the particles during a small shear increment as a function of height in Fig. 1(b). The average particle displacement (dashed red line) increases linearly with height, indicating uniform flow.
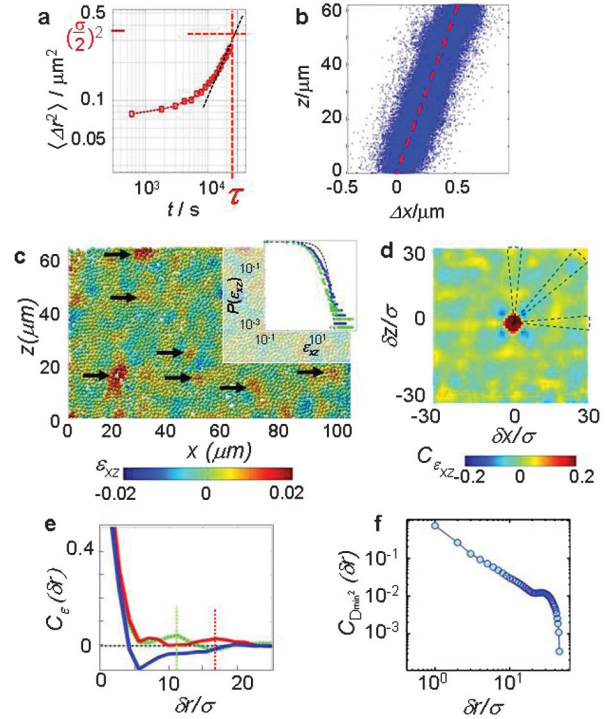

FIG. 1 (color). Homogeneous deformation at a shear rate of $\dot{\gamma} = 1.5 \times 10^{-5}$ s^{-1}. (a) Mean square displacement of the quiescent glass without applied shear. The structural relaxation time τ of the glass is estimated by extrapolating the mean square displacement in the diffusive regime with a line of slope 1 (dashed black line). (b) Displacements of individual particles (+) and average displacement (dashed line) along the shear direction during $\delta t = 10$ min of shear. (c) 7 μm thick reconstruction of the distribution of shear strain after $\delta t = 3$ min of shear. Particle color indicates the value of ϵ_{xz}. The inset in (c) shows the relative frequency of shear strain magnitudes ϵ_{xz} for time intervals $\delta t = 3$ (green stars) and 25 min (blue squares). (d) Angle-resolved spatial correlation $C_{\epsilon_{xz}}$ of the fluctuations of shear strain, in the x-z plane. (e) $C_{\epsilon_{xz}}$ as a function of distance averaged over angular wedges of 10° around the horizontal (red line), the vertical (green line), and the two diagonal directions (blue line). (f) Angle-averaged correlation function $C_{D_{\min}^2}$ as a function of distance in a double-logarithmic representation.

Strong fluctuations exist, however, at the level of the individual particles. We determine values of the local shear strain from the motion of a particle with respect to its nearest neighbors during time intervals of 3 and 25 min and plot the relative frequency of occurrence of shear strain values as a function of shear strain magnitude in Fig. 1(c), inset. For short times, the probability distribution of strain values decreases as a power-law over almost 3 orders of magnitude in probability. Such power-law decay is a fingerprint of highly correlated dynamics [10]. This is also evident from the real-space distribution of the microscopic shear strain ϵ_{xz} [Fig. 1(c)]. Red regions indicate zones where large shear strain is localized and irreversible rearrangements occur, also known as shear transformation

zones [8,9,11]. We determine correlations between these zones by calculating the correlation functions of the shear strain, $C_{\epsilon_{xz}}$, and of the nonaffine displacements, $C_{D^2_{min}}$. At the short time intervals considered here, the correlation functions do not depend significantly on the specific time interval chosen and appear robust. Correlations in the x-z plane are obtained by taking $\delta\mathbf{r} = (\delta x, 0, \delta z)$; a corresponding color-coded representation of the correlation function $C_{\epsilon_{xz}}$ is shown in Fig. 1(d). Remarkably, the correlation function shows a fourfold pattern at its center, which reveals the elastic response of the glass to local shear transformation zones [12]. This glass elasticity leads to strong correlations between shear transformation zones as evidenced by the regular pattern of yellow zones. This is most evident if we average $C_{\epsilon_{xz}}$ within angular wedges around the horizontal, vertical, and diagonal directions and plot the corresponding angle-specific correlation function versus r in Fig. 1(e). The correlation function $C_{D^2_{min}}$ appears to be isotropic. We average over all directions and plot the magnitude of $C_{D^2_{min}}$ as a function of distance in Fig. 1(f). A remarkable power-law decay is observed, which is truncated at the vertical system size $\delta r/\sigma \sim 50$; thus, the correlations span the entire system. We further confirmed that these correlations are independent of the specific measure of nonaffinity by using different definitions of nonaffine motion. The correlation function remained robust. These results provide direct evidence of the existence of long-range strain correlations in a glass, and they highlight the scale-free character of the nonaffine rearrangements that govern plastic deformation. The scale invariance appears to be a generic feature of elastoplastic deformation in other materials, too: The dislocation motion in crystals [10] and the aftershocks in earth quakes [13] display similar scale-free patterns.

We probe these strain correlations by subjecting the glass to increasing shear rates. While the flow remains homogeneous over a range of low strain rates, at a critical strain rate of $\dot{\gamma}_c \sim \tau^{-1}$ we observe a sudden transition to inhomogeneous flow. The glass separates into two bands that flow at different rates, as illustrated by the particle displacements as a function of height obtained at a shear rate of $\dot{\gamma} \sim 1 \times 10^{-4}$ s^{-1} [Fig. 2(a)]. Linear fits to the displacement profile for $z < 23$ μm and $z > 27$ μm [dashed lines in Fig. 2(b)] yield strain rates of 4×10^{-5} and 2.2×10^{-4} s^{-1}, respectively, that differ by a factor of 5. A reconstruction of the shear strain distribution shows that highly nonaffine shear transformation zones accumulate in the upper part [Fig. 2(b)]. We investigate the robustness of the scaling observed in Fig. 1(e) by determining $C_{D^2_{min}}(\delta r)$ separately for the high and low shear bands. The resulting angle-averaged correlation functions are shown together with those of homogeneous flow in Fig. 2(c). A remarkable collapse of the data is observed. While the magnitude of fluctuations in the two bands differs largely,
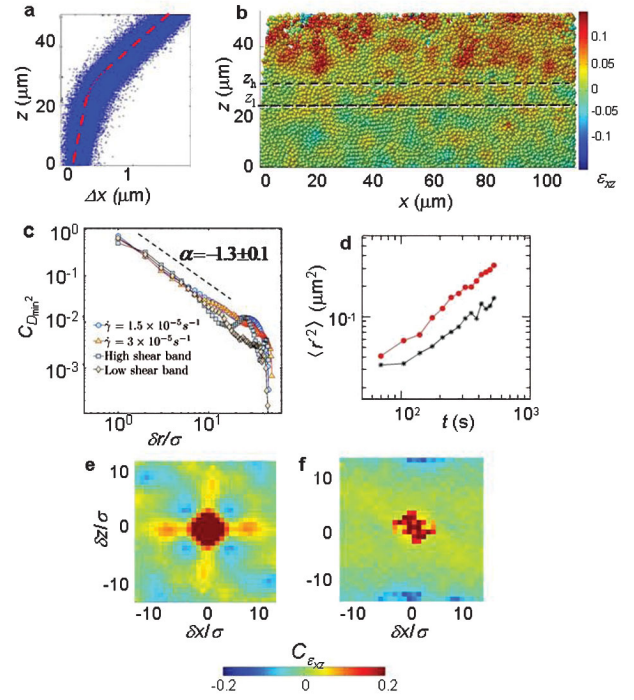

FIG. 2 (color). Inhomogeneous deformation at a shear rate of $\dot{\gamma} = 1 \times 10^{-4}$ s^{-1}. (a) Particle displacements along the shear direction during $\delta t = 4$ min of shear. Dashed red lines are linear fits to the shear profiles for $z < z_l = 23$ μm (low shear band) and $z > z_h = 28$ μm (high shear band). (b) 7 μm thick reconstruction of the distribution of incremental shear strain ϵ_{xz} during the time interval $\delta t = 7$ min. (c) Angle-averaged correlation function $C_{D^2_{min}}$ as a function of distance δr, for the low shear band (blue squares), for the high shear band (yellow diamonds), and for homogeneous shear at $\dot{\gamma} = 1.5 \times 10^{-5}$ (blue dots) and 3×10^{-5} s^{-1} (orange triangles). A least-squares fit to the data gives a slope of $\alpha \sim -1.3 \pm 0.1$ (dashed line). (d) Mean square displacement of particles in the low shear band (black stars and line) and high shear band (red dots and line). (e),(f) Angle-resolved spatial correlations of shear strain, $C_{\epsilon_{xz}}(\delta r)$, in the x-z plane, for the low and the high shear bands, respectively. Correlations are computed over a time interval of $\delta t = 3$ min.

the normalized correlation function shows very similar power-law decay [Fig. 2(c)]: The same scaling exponent applies to the low and the high shear bands, as well as to homogeneous flow. We find a scaling exponent of $\alpha = 1.3 \pm 0.1$ from the best fit to the data. Athermal and quasistatic shear simulations of amorphous solids [14] have shown similar long-range correlations; however, the effect of finite shear rate and finite temperature on the statistical correlations between shear transformation zones remained unclear [15]. Our results conclusively show long-range correlations even at finite shear rate and at finite temperatures.

The difference between the two bands becomes evident when we investigate particle dynamics as a function of time. The mean square displacement of particles around the mean flow, $\langle r'^2(t)\rangle = \langle[\Delta\mathbf{r}(t) - \langle\Delta\mathbf{r}(t)\rangle_z]^2\rangle$, where
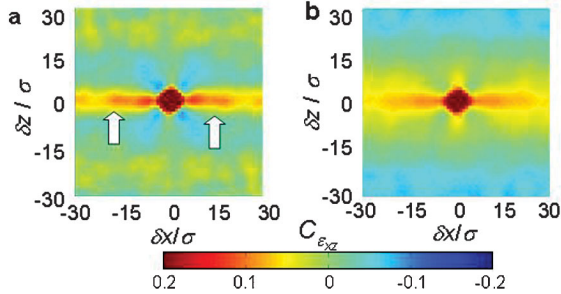
FIG. 3 (color). Evolution of strain correlations during shear band formation. Shear strain correlation functions $C_{\epsilon_{xz}}$ computed for the entire field of view before (a) and after (b) the manifestation of shear bands. The arrows in (a) indicate the strong correlations in the direction of shear that lead to shear banding in later stages (b).

$\langle \Delta \mathbf{r}(t) \rangle_z$ is the average displacement at height z, reveals mobilities in the two bands [Fig. 2(d)] that are larger than those at rest [Fig. 1(a)] and that differ significantly between the two bands. For particles in the high shear band, the mean square displacement is significantly larger, indicating enhanced particle diffusion compared to particles in the low shear band. Remarkably, the strain correlation function $C_{\epsilon_{xz}}$ calculated separately for both bands [Figs. 2(e) and 2(f)] reveals a spatial symmetry change. While for the low shear band, the central fourfold symmetry is still predominant [Fig. 2(e)], for the high shear band, this symmetry is lost, and the pattern appears isotropic [Fig. 2(f)]. This symmetry change reflects the transition from a solid to a liquidlike response of the glass. These results highlight the central importance of strain correlations: While the transition from a reversible elastic to an irreversible viscous response is usually associated with a symmetry change in time, our results show that this transition is also associated with a spatial symmetry change in the strain correlation function, underlining its fundamental character. A similar interpretation is given to fracture surfaces of metallic glasses that display striking evidence of such a solid-to-liquid transition [16]. Our colloidal glass allows us to directly visualize the strain correlations and identify their central importance in this solid-to-liquid transition.

How does this transition emerge? To elucidate this, we follow correlations during the initial stages of shear banding. We determine strain distributions during the transient stages, before shear bands manifest, and calculate correlation functions for the entire field of view [Figs. 3(a) and 3(b)]. In the early stage, the correlation shows a strong bias in the horizontal direction (arrows). This horizontal bias signals the excitation of additional elastic modes at higher shear rates that cause strong correlations between shear transformation zones in the horizontal direction. This bias lowers the effective resistance to flow in the direction of shear, thereby leading to shear bands in the later stages of deformation [Fig. 3(b)]. These results highlight the

importance of long-range correlations in the shear banding of glasses. Shear experiments at much higher shear rates show that shear bands can originate from density fluctuations [17]. The model proposed by the authors suggests a linear viscous flow at very low shear rates that is hard for them to address experimentally. Here, we have successfully addressed this low shear rate regime; our measurements at the onset of shear banding show strong changes in the correlations of microscopic strain but no measurable dilatancy.

Our results establish the existence of long-range strain correlations in the flow of glasses. The long-range elastic interactions between shear transformation zones lead to scale-free deformation of the glass. While our results for shear banding are obtained for colloidal glasses, they should be generic to glassy flows [18]. The formation of shear bands has often been linked to strain softening of the material, caused by excess dilation, that accompanies the formation of shear transformation zones [8,17]. The direct imaging of strain correlations that we have reported here demonstrates that long-range elastic correlations play a central role in the manifestation of such instabilities [19]. Finally, the robust scaling that we observe suggests a naturally scale-free flow and relaxation of glasses. We propose similar analysis of shear flows in systems like granular, foams, and emulsions to test the universality of the scaling exponent and to determine the universality class of the flow and relaxation of amorphous materials.

[1] C. A. Angell, Science **267**, 1924 (1995); P. G. Debenedetti and F. H. Stillinger, Nature (London) **410**, 259 (2001).
[2] G. Adam and J. H. Gibbs, J. Chem. Phys. **43**, 139 (1965).
[3] C. Donati, S. C. Glotzer, and P. H. Poole, Phys. Rev. Lett. **82**, 5064 (1999); C. Bennemann, C. Donati, J. Baschnagel, and S. C. Glotzer, Nature (London) **399**, 246 (1999).
[4] L. Berthier, G. Biroli, J.-P. Bouchaud, L. Cipelletti, D. El Masri, D. LHote, F. Ladieu, and M. Pierno, Science **310**, 1797 (2005); E. R. Weeks, J. C. Crocker, and D. A. Weitz, J. Phys. Condens. Matter **19**, 205131 (2007).
[5] C. E. Maloney and M. O. Robbins, Phys. Rev. Lett. **102**, 225502 (2009); S. Maccarrone et al., Soft Matter **6**, 5514 (2010); P. Olsson and S. Teitel, Phys. Rev. Lett. **99**, 178001 (2007).
[6] E. R. Weeks, J. C. Crocker, A. C. Levitt, A. B. Schofield, and D. A. Weitz, Science **287**, 627 (2000).
[7] P. N. Pusey and W. van Megen, Nature (London) **320**, 340 (1986); Phys. Rev. Lett. **59**, 2083 (1987).
[8] F. Spaepen, Acta Metall. **25**, 407 (1977); A. S. Argon, Acta Metall. **27**, 47 (1979).
[9] M. L. Falk and J. S. Langer, Phys. Rev. E **57**, 7192 (1998).

[10] M.-C. Miguel, A. Vespignani, S. Zapperi, J. Weiss, and J.-R. Grasso, Nature (London) **410**, 667 (2001); J. Weiss and D. Marsan, Science **299**, 89 (2003); D. M. Dimiduk, C. Woodward, R. LeSar, and M. D. Uchic, Science **312**, 1188 (2006).

[11] P. Schall, D. A. Weitz, and F. Spaepen, Science **318**, 1895 (2007).

[12] J. D. Eshelby, Proc. R. Soc. A **241**, 376 (1957); G. Picard, A. Ajdari, F. Lequeux, and L. Bocquet, Eur. Phys. J. E **15**, 371 (2004).

[13] D. Marsan and O. Lengliné, Science **319**, 1076 (2008); D. Marsan, C. J. Bean, S. Steacy, and J. McCloskey, J. Geophys. Res. **105**, 28 081 (2000).

[14] C. Maloney and A. Lemaitre, Phys. Rev. Lett. **93**, 016001 (2004); Phys. Rev. E **74**, 016118 (2006).

[15] A. Lemaitre and C. Caroli, Phys. Rev. Lett. **103**, 065501 (2009); H. G. E. Hentschel, S. Karmakar, E. Lerner, and I. Procaccia, Phys. Rev. Lett. **104**, 025501 (2010).

[16] F. Spaepen, Acta Metall. **23**, 615 (1975).

[17] R. Besseling, L. Isa, P. Ballesta, G. Petekidis, M. E. Cates, and W. C. K. Poon, Phys. Rev. Lett. **105**, 268301 (2010).

[18] P. Schall and M. van Hecke, Annu. Rev. Fluid Mech. **42**, 67 (2010).

[19] V. V. Bulatov and A. S. Argon, Model. Simul. Mater. Sci. Eng. **2**, 167 (1994).